Rare-region onset of superconductivity in niobium nanoislands

Malcolm Durkin,[1] Rita Garrido-Menacho,[1] Sarang Gopalakrishnan,[2] Narendra K. Jaggi,[3] Ji-Hwan Kwon,[4] Jian-Min Zuo,[4] and Nadya Mason[1]

[1]*Department of Physics and Frederick Seitz Materials Research Laboratory, University of Illinois at Urbana-Champaign, Urbana, Illinois 61801, USA*

[2]*Department of Engineering Science and Physics, College of Staten Island, Staten Island, New York 10314, USA and Initiative for the Theoretical Sciences, CUNY Graduate Center, New York, New York 10016, USA*

[3]*Department of Physics, Illinois Wesleyan University, Bloomington, Illinois 61702, USA*

[4]*Department of Materials Science and Frederick Seitz Materials Research Laboratory, University of Illinois at Urbana-Champaign, Urbana, Illinois 61801, USA*

(Received 23 April 2019; revised manuscript received 26 November 2019; published 10 January 2020)

We report measurements of the superconducting properties of isolated Nb nanoislands (600–2500 nm diameters) and explain their unusual behavior in terms of rare-region onset effects, predicted for random metal-superconductor granular systems [B. Spivak, P. Oreto, and S. A. Kivelson, Phys. Rev. B **77**, 214523 (2008)]. We find that the island T_c is strongly suppressed even at large island diameters, exceeding 1 μm. This behavior is unexpected given that conventional theories of superconductivity in small grains predict suppression of T_c only at a length scale that is two orders of magnitude smaller. In addition, we observe large island-to-island variations in T_c for nominally identical islands. These two experimental observations, coupled with direct measurement of grain distribution using transmission electron microscopy, conductive atomic force microscopy, and computer simulations, provide evidence for our picture in which the onset of superconductivity on an island coincides with the transition temperature of its largest constituent grain, and then spreads to other grains due to proximity coupling.

DOI: 10.1103/PhysRevB.101.035409

I. INTRODUCTION

An ongoing question in physics is, What determines the critical behavior of disordered systems? Recent evidence has suggested that many disordered systems—from metals [1] to magnets [2] to a wide variety of superconductors [3–9]—might be dominated by the behavior of "rare regions" of a correlated phase, which control the inception and dynamics of bulk electronic phases. Disorder is present at the microscopic level in all physical systems. In typical three-dimensional systems, this microscopic disorder averages out when computing macroscopic, long-wavelength response properties. However, in many low-dimensional correlated phases of matter, even moderate microscopic disorder can have drastic implications for macroscopic transport: examples include Anderson localization even in the presence of weak disorder in one or two dimensions (2D) [10], 2D quantum metals [3,5,9,11], quantum Griffiths phases [7], and related states. In many of these examples, disorder does not "self-average" on large scales: the large-scale properties of the material are determined, not by its *typical* parameter values, but by regions with anomalous parameters (i.e., rare regions) that have an outsize effect on response. Experimentally, rare-region effects are often inferred from macroscopic measurements; experimentally identifying the microscopic spatial distributions of local parameters has only been feasible in a few cases.

The superconductor-metal-insulator transition in disordered superconducting thin films is believed to exhibit strong rare-region effects. In superconducting thin films, increasing disorder is predicted to generate a continuous quantum phase transition between a superconducting and insulating state, as the normal state resistance (a proxy of disorder) approaches the quantum of resistance ($R_Q \sim 6.4\,\mathrm{k\Omega}$) [12]. However, multiple experiments have instead demonstrated that superconductivity is suppressed at much lower values of the film resistance and phase transitions to low-resistance metals [11,13,14]. The main theoretical paradigm for understanding such superconductor-metal-insulator transitions [3–5] assumes that the films possess emergent inhomogeneity, i.e., they break up into locally superconducting islands in a metallic matrix.

While early quantitative studies of inhomogeneous superconductors focused on percolating networks of weakly coupled superconducting grains embedded in nonmetallic matrices [15,16], very low-resistance granular films, where superconducting grains are embedded in a metal, have not been well studied experimentally, and a direct connection with pertinent theoretical work [3] has not been attempted. In the well-coupled regime, randomness in grain size dominates, and global superconductivity appears rapidly after the transition of the largest superconducting grain (i.e., a rare region). This type of low-resistance, highly inhomogeneous superconductivity has been invoked to explain many recent experimental results [6–9,17], and rare superconducting domains have been observed above the superconducting transition in NbN [18]. However, these works did not connect the observed behavior to the distribution of grains, or to any specific theory of rare-region onset of superconductivity.

In previous work [19], we studied arrays of Nb islands on Au films, finding anomalous island T_c dependence on the strength of coupling between islands. In this paper, we present measurements performed on individual islands, eliminating the coupling between islands. We find that the T_c of these islands is strongly suppressed, even for island diameters of over 1200 nm, diameters much larger than the 260 nm that had been used in our previous study of island arrays. This behavior is unexpected given that conventional theories of superconductivity in small grains [20] predict suppression of T_c only at a length scale that is two orders of magnitude smaller, which is consistent with previous experiments on isolated superconducting grains [21–23]. In addition, we observe strong island-to-island fluctuations of T_c for a broad range of island diameters. This paper presents data for the temperature-dependent resistance, R(T), of a broad range of islands and their detailed materials characterization, especially a direct measurement of the grain-size distribution using conductive atomic force microscopy (c-AFM). Guided by Spivak *et al.* [3], we use a combination of experimental results and computer simulations to provide a picture for the emergence of superconductivity in this system using the concept of rare-region onset.

II. EXPERIMENTAL METHODS

Islands were composed of 70-nm-thick electron-beam evaporated Nb, on top of insulating SiO_2 substrates, and had diameters varying between 600 and 2500 nm [Fig. 1(a)]. Nb was chosen because it forms nanoscale grains when either sputtered or evaporated, with structure and grain size dependent on deposition parameters [24]. We patterned our samples using electron-beam lithography on Poly(methyl methacrylate) (PMMA), electron-beam evaporation, and lift-off processes all on a silicon wafer with a 300-nm oxide layer. We first made the four-point contacts, which consist of 1 nm of Ti and 10 nm of Au. Then we patterned a Nb island on top of the normal metal contacts. Nb was deposited in an ultrahigh vacuum system with a 67-cm throw distance. A brief ion mill was performed prior to electron beam evaporating 70 nm of Nb at a pressure of 1.0×10^{-9} Torr or less. The Au contacts had a 50–100-nm overlap underneath the Nb island. The sample was then placed in a chip carrier, contacted with a wedge bonder, and measured in a 1 K cryostat using standard lock-in amplifier techniques.

III. EXPERIMENTAL MEASUREMENTS

We measured R(T) for scores of islands, of varying diameters. Each panel in Figs. 1(b)–1(h) shows R(T) for approximately ten islands, all having the same thickness, the same diameter, and grown on the same chip, under identical conditions, and measured in the same run. While each island has a well-defined and stable (reproducible) "onset" temperature, as indicated by the sudden decrease in resistance, this onset temperature is different for different islands of nominally the same diameter. For example, for the set of islands with a diameter of 600 nm, the onset T_c varies from 2.6 to 5.1 K, even though their thickness and diameter are within a few percent of each other. The amount of this unusually large island-to-island variation of the onset T_c decreases as the diameter

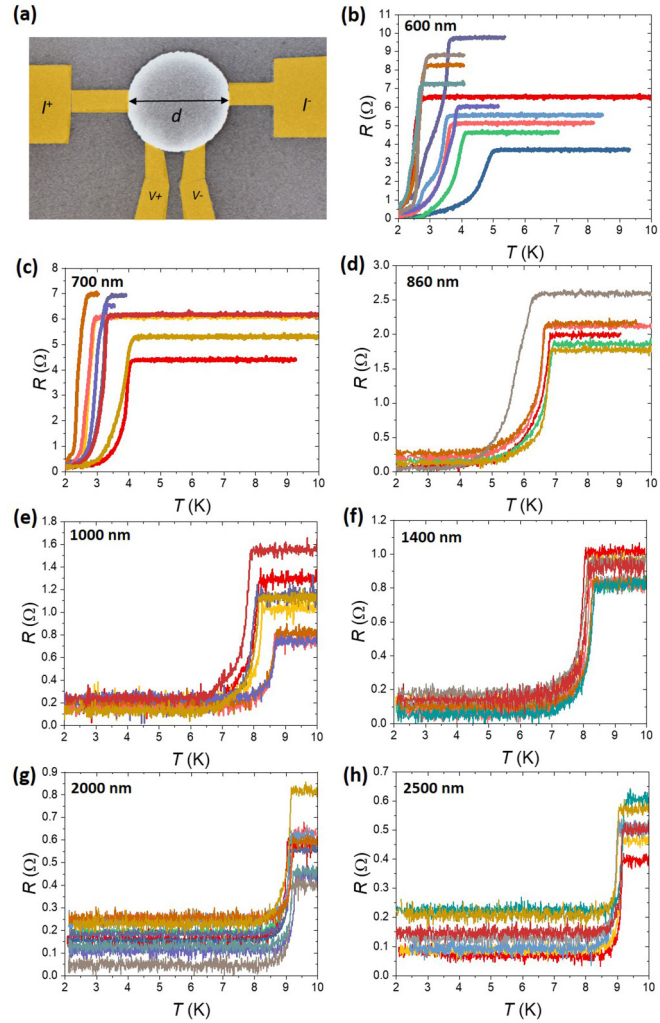

FIG. 1. Representative scanning electron microscopy (SEM) device image and island-to-island fluctuations of T_c for various island diameters. (a) False-color SEM image of island and leads (yellow) where d is island diameter. Resistance versus temperature data for island diameters of (b) 600, (c) 700, (d) 860, (e) 1000, (f) 1400, (g) 2000, and (h) 2500 nm. Each R(T) panel contains temperature sweeps for 8–12 island devices.

increases, but it clearly persists at least up to a diameter of 1400 nm, as shown in the other panels of Fig. 1. These data suggest that the onset behavior of each island might be dominated by some specific and frozen nanoscale feature of that particular island, a feature that is at a scale much less than that of the island diameter.

To show the important and reproducible observed trends for the superconducting transitions in this system, we have summarized in Fig. 2 data for seven sets of samples that were prepared under slightly different evaporation conditions. Each evaporation run evaluated measured 5 to 12 islands of the same diameter (except for E1–E3 where only one island per diameter was evaluated). Figure 2(a) shows the dependence of the mean T_c upon the diameter of the island. The curves all show the same qualitative behavior: T_c is strongly suppressed as diameter is decreased below $\sim 1\,\mu$m. For large islands ($>2\,\mu$m), T_c approaches the bulk value for Nb, 9.1 K.

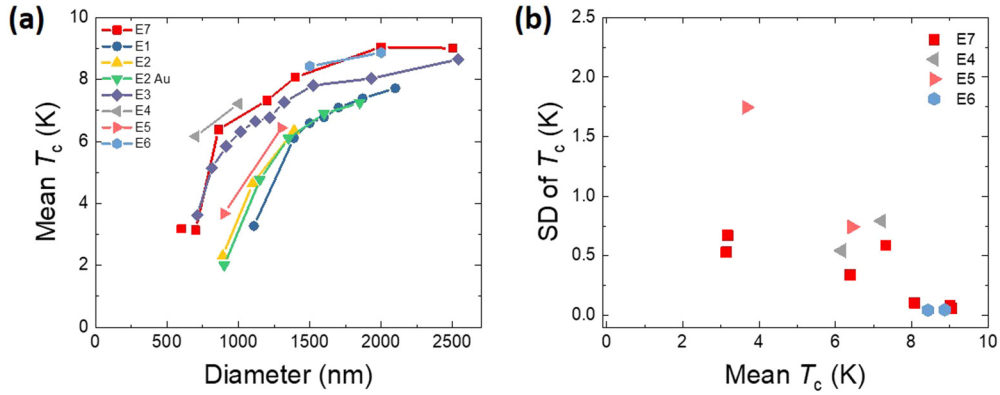

FIG. 2. Superconducting transition for different island sizes across various evaporation runs. (a) Mean T_c as a function of island diameter. Different colors denote different Nb evaporation runs. Each evaporation run evaluated measurements of 5 to 12 islands of the same diameter (except for E1–E3, where only one island per diameter was evaluated). The samples indicated by E2 Au have underlying Au. E3 was obtained using a lower evaporation pressure. (b) Standard deviation of the island-to-island variation of T_c for evaporations 4–7 (E4–E7).

However, as the island diameter is decreased, T_c drops sharply, to below 4 K at 1 μm, and well below that for smaller diameters. To summarize the observed behavior of island-to-island fluctuations, we show in Fig. 2(b) the standard deviation of T_c versus the corresponding mean value of T_c for four sets of samples (E4–E7) for which 5 to 12 islands of the same diameter were measured. Over the range of diameters explored in this study, these island-to-island fluctuations increase as island diameter decreases.

The set labeled E2 Au in Fig. 2 shows that data for islands on gold squares are nearly identical to islands placed on insulators as shown by sets E1–E7. This demonstrates that the normal metal (either underlying, or in the leads) is not the reason for suppression of the transition temperature. The micron-length scales at which superconductivity is suppressed in these islands are far longer than other length scales related to superconductivity in Nb, such as the coherence length (∼29 nm) [19] or the scale at which the gap equals the discrete energy-level spacing (∼4 nm) [21,24].

We note that qualitatively similar size dependence of T_c in Nb nanostructures and films has been observed in past works [25–27]. They found that submicron niobium structures patterned with ordinary PMMA resist had a significantly suppressed T_c compared to the T_c of coevaporated Nb structures patterned using MMA/PMMA, ZEP520A, and ZEP520A with Ti passivation.

Because of the technological importance of Nb-based superconducting nanowire single-photon detectors, these size-dependence effects are well documented and various fabrication techniques to improve the T_c of Nb nanowires have been explored [25–27]. But, the underlying physical mechanism has not been studied previously. In addition, the most interesting experimental features, e.g., the very large island-to-island fluctuation of T_c and their systematic dependence on island diameter, have not been reported in past works. This paper provides comprehensive data, detailed materials characterization, and finds semiquantitative agreement of the data with computer simulations based upon a particular theory [3]. Altogether it builds an intuitively transparent picture for the emergence of superconductivity in this system using the concept of rare-region onset.

IV. DISCUSSION

A. Materials characterization

1. Transmission electron microscopy characterization of grains

Figure 3 shows typical transmission electron microscopy (TEM) images of our Nb islands, where black crystals (the "grains") are surrounded by gray, amorphouslike material. Top-view TEM measurements were performed on Nb islands placed on TEM windows, which consist of a 20-nm-thick SiO_2 membrane. The horizontal measurements were performed by cutting an island cross section using a focused ion beam and performing a cross-sectional TEM. The TEM characterization shows that the grains are columnar in shape, suggesting that one could regard each island as a two-dimensional array of columnar grains.

The grain-size statistics were extracted from top-view TEM images using an object finder, which applied a low-pass filter for smoothing and then identified grains as areas where the image intensity is below a threshold. Using Fig. 3(a), which has high-contrast regions visible in both light and dark, we executed the described image-processing steps followed

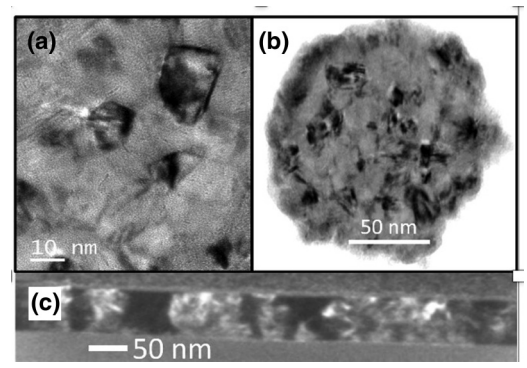

FIG. 3. TEM images showing film morphology. (a) Zoomed-in TEM image showing crystalline Nb grains in black and an amorphouslike metallic phase of Nb in gray. (b) TEM of a 130-nm-diameter Nb island. TEM images in (a) and (b) were performed on 30-nm-thick Nb. (c) Cross-sectional TEM (dark field) performed on 70-nm-thick Nb showing columnar grains.

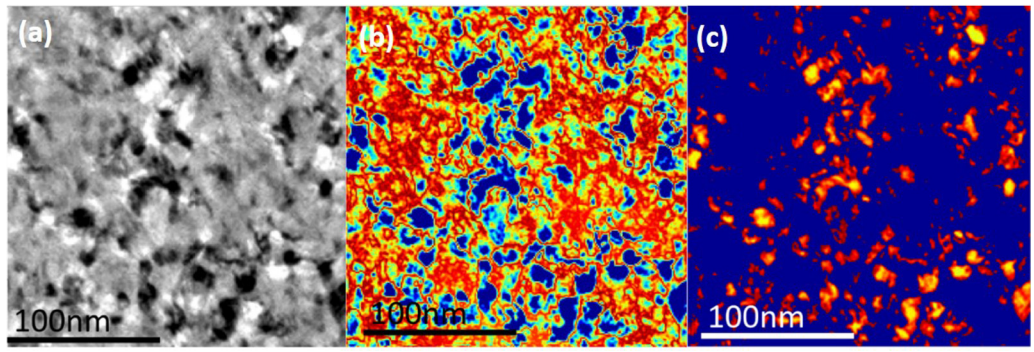

FIG. 4. TEM image processing used to extract grain-size distribution. (a) Raw TEM image of a Nb film. High-contrast grains are visible in both black and white. (b) The TEM image after a low-pass filter has been applied, mean intensity is subtracted, and the absolute value is taken. High-contrast grains appear in blue. (c) High-contrast grains identified by the object finder are shown in red and orange.

by the threshold identification. These image-processing steps are shown and articulated in the figure captions for Figs. 4(a)–4(c). As can be seen in Fig. 5, analysis of these TEM images showed an *exponential distribution* of grain diameters L, $P(L, \beta) = \beta e^{(-\beta L)}$ with $\beta = 0.243\,\mathrm{nm}^{-1}$ giving a mean grain diameter of 4.12 nm.

2. Conductive AFM characterization of grains

Conductive atomic force microscopy involves performing contact-mode AFM measurements using a conducting cantilever and dragging the cantilever across a sample as depicted in Fig. 6(a) inset. The tip is held at a constant bias, the sample is grounded at the other end of the chip, and the current is measured. Due to the narrow tip, the current measured is sensitive to the conductance near the tip. A resistor network simulation seen in Fig. 6(a) shows current peaks when the tip is above highly conductive regions. Figure 6(b) shows the results of conductive AFM measurements performed on 70-nm-thick Nb films, where a distribution of current peaks is evident. The size of these current peaks was extracted using an object finder and, as can be seen in Fig. 6(c), corresponds to a distribution of grain diameters L, $P(L, \beta) = \beta e^{(-\beta L)}$ with $\beta = 0.122\,\mathrm{nm}^{-1}$ giving a mean grain diameter of 8.2 nm. This

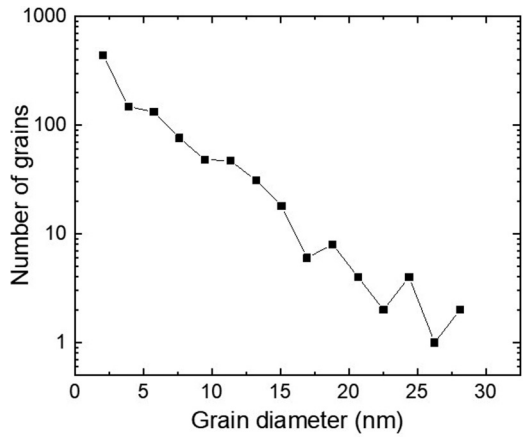

FIG. 5. TEM grain-size distribution. Histogram of Nb grains extracted using TEM demonstrating an exponential distribution of grains. The fitted mean grain diameter is 4.12 nm.

exponential distribution is similar to the exponential distribution of grains found using TEM. These two results together clearly show that the film consists of highly conductive grains embedded in a second amorphouslike phase that is *metallic*, with a higher resistivity.

While c-AFM and TEM data confirm the *exponential nature of grain-size distribution* of the crystalline Nb grains, there is a discrepancy of approximately a factor of 2 in the mean size of these crystallites. This discrepancy can be understood by the fact that the c-AFM measures conducting regions—which may contain small clusters of nearly touching grains—while the TEM measures each individual grain. In particular, the factor of 2 discrepancy implies that there are multiple clusters of 2–3 small grains (which is also evident by eye in the TEM data). Because what is pertinent for our analysis is the size of individual grains, the grain-size distribution extracted from TEM data is the most relevant and is used for the theoretical analysis.

3. Combined AFM, energy-dispersive x-ray, Rutherford backscattering, TEM, and XRD characterization of the amorphouslike material

We characterize the amorphouslike Nb phase in the patterned islands based upon a combined analysis of AFM, energy-dispersive x-ray (EDX), Rutherford backscattering (RBS), TEM, and x-ray diffraction (XRD) data. These data confirm that the amorphous phase is metallic, and that it has a resistivity much higher than that of crystalline Nb. We have evidence that it is not crystalline Nb oxide, it is likely a mixture of amorphous and nanocrystalline Nb phases, and that its formation is related to the outgassing from the PMMA resist during processing. In this section, we summarize the observations that lead to the above conclusion.

RBS data on patterned films fit quite well to a model consisting of the expected 70-nm Nb film on a 300-nm SiO_2/Si substrate, but there are small systematic regions of misfit suggesting the incorporation of a small amount of some other element into the film. Modifying the model to include any oxygen within the film makes the RBS fits worse, and we therefore believe that we can rule out any significant amount of NbO_x. EDX shows small amounts of carbon, but, as always, it is difficult to tell if the carbon is incorporated into the film, or if it is a surface contamination.

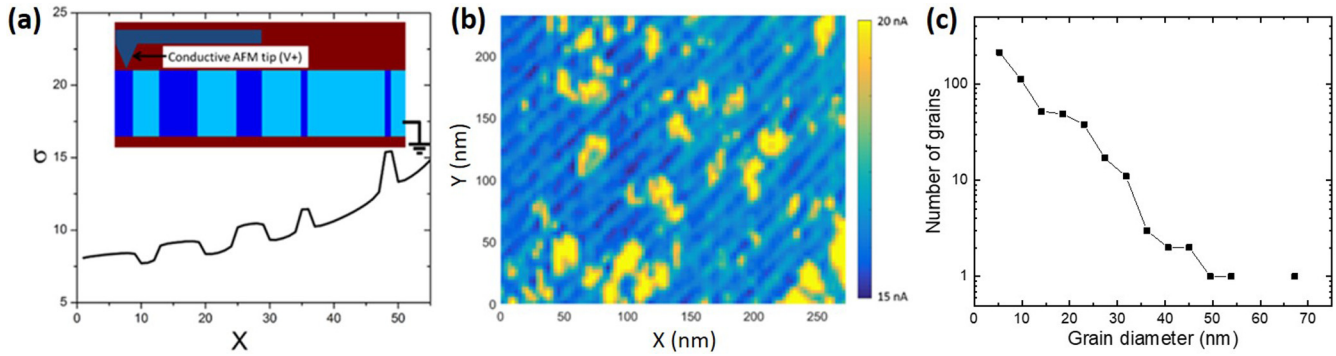

FIG. 6. Conductive AFM and its use to extract grain-size distribution. (a) Inset shows a model granular film with columnar features similar to those observed in our system. Blue corresponds to low resistances, light blue corresponds to intermediate resistances 3 times higher, and red corresponds to insulating. The plot shows simulated conductance as the tip is dragged along these features. (b) A conductive AFM measurement of a Nb film with fixed bias voltage. Current peaks are visible with width comparable to that of the grains. (c) Histogram of conductive AFM grains extracted with an object finder. The fitted mean grain diameter is 8.2 nm.

XRD measurements were performed on Nb films which were e-beam evaporated under similar conditions as our Nb islands. A conventional $2\theta/\omega$ XRD scan as well as glancing XRD scan were performed on these films and it was found that besides Nb and Si (substrate), no other crystalline materials were present on the film. The widths of the Nb peaks seen in the XRD spectra gave insight into the crystalline size. The estimated average crystalline size from the XRD results is about 9.7 nm, which is qualitatively consistent with the c-AFM measurements. Because the islands are very thin (70-nm thickness) and small (few hundred nm in diameter), and because the second phase is amorphous, as shown by TEM, we were unable to unambiguously identify the chemical composition of this second amorphouslike Nb-based phase using XRD.

For the purposes of our theoretical model, all that is necessary is for the second phase to be metallic; whether it is crystalline or amorphous is not relevant to the theoretical model. That the second phase is indeed metallic is convincingly demonstrated by c-AFM as discussed previously. Scanning electron nanodiffraction using TEM [28] (Fig. 7), however, does provide evidence that the gray regions in the TEM images indeed have an amorphouslike character, whereas the dark grains are pure crystalline Nb.

B. Theoretical model of superconducting behavior

The key theoretical idea invoked to explain the superconducting properties of this granular metal-superconductor system is the following: The temperature T_c for the onset of superconductivity in any particular island coincides with the superconducting transition of its *largest* constituent grain. Since this is the transition temperature of a grain embedded in a metallic matrix, formed by the amorphouslike phase, superconductivity occurs when the pairing energy scale Δ is greater than the Thouless energy $E_{\rm Th} \sim \hbar D/L^2$, where L is the grain diameter and D is the electronic diffusion constant [29]. In other words, the time an electron dwells on a grain before diffusing out, $t_{\rm Th} = \hbar/E_{\rm Th}$, must be longer than the time it takes to form superconducting correlations, $t_\Delta = \hbar/\Delta$. Taking the standard dirty-limit $\Delta \approx \hbar D/\xi_{\rm SC}^2$, where $\xi_{\rm SC}$ is the superconducting coherence length. This criterion of $t_{\rm Th} > t_\Delta$ implies that T_c is suppressed when the grain diameter $L \sim \xi_{\rm SC}$. This mechanism is different from those found in superconducting grains embedded in insulators, where electrons do not diffuse out of the grain and T_c is only suppressed when Δ is on the order of the single-particle level spacing of the grain [21].

In this extremal-grain model, larger islands have higher T_c than smaller islands because they have more grains and, therefore, a higher probability of having an anomalously large, high-T_c grain. For the parameters in our experiments, and

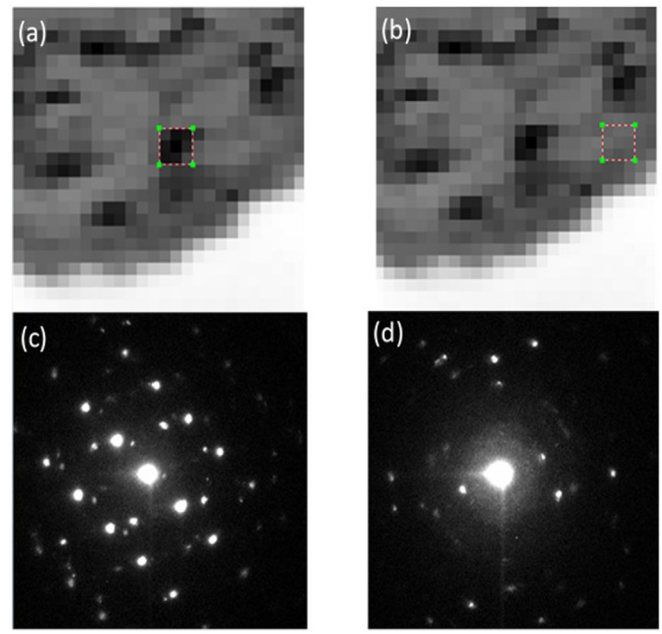

FIG. 7. Virtual bright-field TEM images and selective area diffraction patterns. (a), (b) Virtual bright-field TEM image of a 104-nm-square region of a Nb island obtained using scanning electron nanodiffraction with a step size of 4 nm [28], with two different selected areas identified by 9-pixel squares (12 nm by 12 nm) in each case. (c), (d) Diffraction patterns from the two corresponding areas (a) and (b), respectively. (c) Sharp diffraction spots, corresponding to highly crystalline Nb in the dark grains. (d) Combination of a diffuse halo, a signature of an amorphous component, and some spots corresponding to a nanocrystalline/amorphous phase.

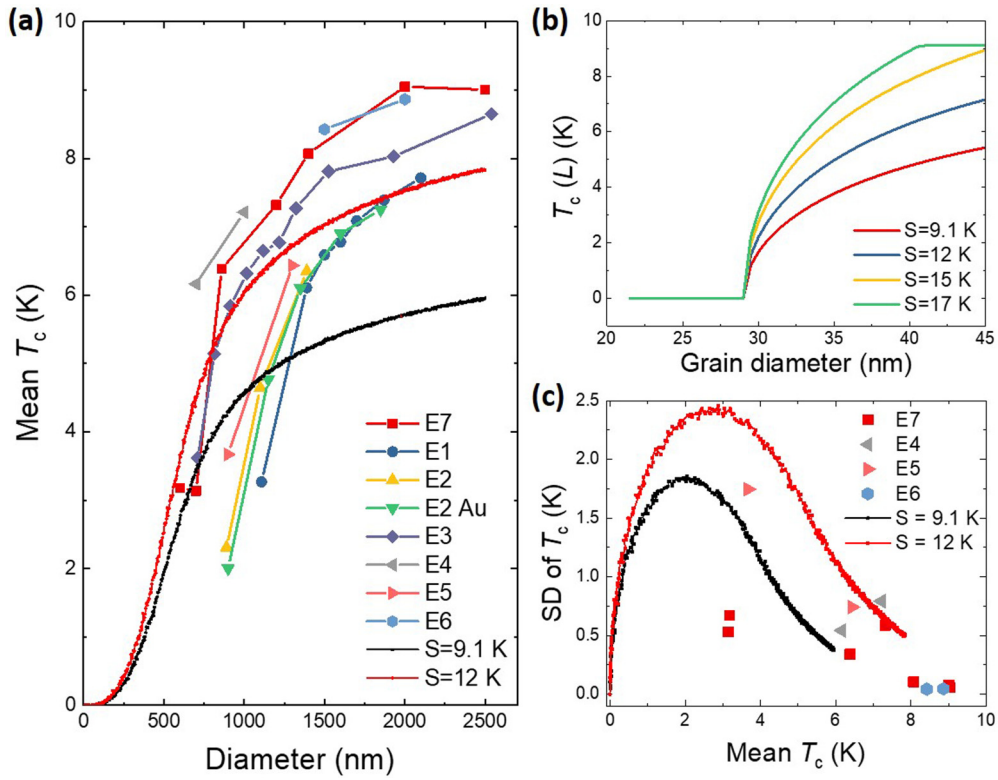

FIG. 8. Extremal-grain model. (a) Simulated grain sizes are applied to Eq. (2) to obtain an estimate of T_c as a function of island diameter. Mean simulated T_c for two S values (black and red curves) is shown alongside data from evaporations 1–7 (E1–E7). (b) Grain critical temperature $T_c(L)$ as a function of grain diameter as S is varied in Eq. (2). (c) Simulated standard deviation as a function of mean T_c for the two same S values (black and red) shown alongside evaporations 4–7 (E4–E7).

given the exponential probability distribution of grain sizes, an overwhelming fraction of the grains are smaller than the coherence length ξ_{SC}. Under these conditions, as indicated in the Appendix, the theory of Spivak *et al.* [3] yields $T_c\,(L) \sim \sqrt{L - \xi_{sc}}$ when L is close to but exceeds ξ_{SC}. If we also assume that the grain's $T_c\,(L)$ should saturate at the bulk value of T_{c0} as $L \gg \xi_{SC}$, the simplest expression for $T_c\,(L)$ that is consistent with these requirements is

$$T_c(L) = 0 \quad \text{for } L < \xi_{SC}$$
$$T_c(L) = T_c^0\sqrt{1 - \frac{\xi_{SC}}{L}} \quad \text{for } L > \xi_{SC}, \tag{1}$$

where T_c^0 is the bulk transition temperature of Nb, 9.1 K, and ξ_{SC} is the Ginzburg-Landau dirty-limit superconducting coherence length of Nb.

In our system, grain size has a probability distribution, $P(L)$, where L is the grain diameter. This distribution was determined *experimentally* as $P(L\beta) = \beta e^{(-\beta L)}$ with a value $\beta = 0.24\,\text{nm}^{-1}$ according to the TEM analysis, for one of the thin films characterized in detail. This corresponds to a mean grain diameter, β^{-1}, of 4.12 nm for this value of β. As mentioned at the end of Sec. IV A 2, because what is pertinent for our analysis is the size of individual grains, the grain-size distribution extracted from TEM data is the most relevant and is used for the theoretical analysis.

An island of diameter d has, on an average, $N \sim \rho\pi d^2/4$ grains of varying sizes, where ρ is the number density of grains. The grain density ρ depends upon two factors, the mean grain diameter β^{-1}, and f, the area fraction of the island that is occupied by crystalline Nb, $(1-f)$ being the area fraction covered by the second amorphouslike phase. In principle, both parameters β and f can vary depending upon the deposition and processing conditions such as chamber pressure, resist used, substrate temperature, technique used for Nb deposition (e-beam evaporation vs sputtering, for example), etc.

C. Simulations of extremal-grain model

The simulation proceeds as follows: It determines N, the expected average number of Nb grains on one island (this depends upon the island diameter d, β, and f). It then draws N grains from the distribution $P(L, \beta) = \beta e^{(-\beta L)}$ and finds $L_{\max}$, the largest grain diameter in that set. From this the island T_c is computed using Eq. (1) with $L = L_{\max}$. This process was repeated for 4000 islands of the same diameter. The corresponding 4000 values of island T_c are used to compute the mean T_c and the standard deviation of T_c for that particular value of island diameter. The computed results for this model are shown in Fig. 8 and compared with our key experimental results.

Out of the three parameters introduced so far for this model (ξ_{SC}, β, f), two are known to us with some confidence. β , which is related to the mean grain size, is experimentally determined (via TEM) to be $0.24\,\text{nm}^{-1}$. ξ_{SC} is the Ginzburg-Landau dirty-limit superconducting coherence length of Nb, which was estimated in our previous study of arrays of Nb

islands to be approximately 29 nm [19], although it can vary depending upon the deposition conditions and the purity of the films. $(1-f)$ is the area fraction of the island that is covered by the second amorphouslike metallic phase. So, the parameter f can, in principle, vary substantially with the kind of resist used, the deposition conditions, etc., and it can even be correlated with the island diameter; however, we find that the overall dependence of mean T_c and the standard deviation of T_c as a function of island diameter is rather weakly dependent upon the specific value of f. Although we do not have direct experimental measures on the value of f for the full range of our samples, we can place limits on the range over which it can vary by an analysis of the normal-state resistance using a percolation model. Our random resistor network analysis, discussed in the next section, suggests that f is less than 0.6, which is consistent with c-AFM analysis. For the smallest islands, where interactions with the products of outgassing from PMMA can be quite large, f could be smaller. Simulations indicated by black points in Figs. 8(a) and 8(c), and labeled by $S = 9.1$ K, correspond to this particular constrained case, with $\beta = 0.24\,\mathrm{nm}^{-1}$, $\xi_{SC} = 29$ nm, and values of f that are correlated with the island diameter (smaller area fraction of Nb grains for smaller diameters.)

We note that simulation results for this constrained case are in semiquantitative agreement with the major aspects of the observed results. The overall shape of the observed behavior of mean T_c as a function of island diameter is captured correctly by the simulations. This includes the suppression of T_c below 1400 nm and the saturation of T_c at large diameters. As shown in Fig. 8(c), the experimentally observed increase of standard deviation of T_c for smaller values of mean T_c is correctly predicted by the model, as is the approximate magnitude of these island-to-island variations in T_c.

Even though this constrained model accounts for key features of the data, it is clear from Fig. 8 that the computed results show deviations from the experimental results. We thus consider the effects of varying parameters to obtain better agreement. A straightforward variant is to assume that grain T_c (L) increases much more rapidly for $L > \xi_{SC}$, but it does not exceed the bulk value of T_c. Thus, we can normalize by a factor S rather than by 9.1 K as shown in Eq. (2).

$$T_c(L) = 0 \quad \text{for } L < \xi_{SC}$$
$$T_c(L) = \min\left[9.1,\ S\sqrt{1-\frac{\xi_{SC}}{L}}\right] \quad \text{for } L > \xi_{SC}. \qquad (2)$$

The effect of varying the S parameter is indicated in Fig. 8(b). Increasing S has the effect of narrowing the window of grain diameters that will produce a T_c *between* 0 and 9.1 K. For $S = 12$ K, the grain sizes playing a role in the transition are between 29 and 45 nm as shown in Fig. 8(b). At larger grain diameters, the grain T_c saturates to the bulk value of 9.1 K, as one would expect. Stated differently, this corresponds to the assumption that grains above 45-nm diameter have an onset T_c that equals the bulk T_c, possibly because they experience additional proximity coupling. The traces labeled $S = 12$ K in Fig. 8 show the simulation results (red points) based upon Eq. (2). While this gives a much better agreement for the numerical values of mean T_c, and for the overall trend of T_c as a function of diameter, than that predicted by $S = 9.1$ K, the agreement with the observed behavior of standard deviation of T_c versus the corresponding mean value of T_c is worse.

One can consider all four parameters of the model (ξ_{SC}, β, S, f) as being adjustable, to some extent, and explore if that might yield simultaneous agreement with all aspects of the data. It might also provide an explanation for the dependence of the trends upon deposition conditions (for example, quality of the chamber vacuum, deposition technique, resist used).

(1) β, which is related to the mean grain size, can, in principle, depend upon deposition conditions. But, the computed results are extremely sensitive to the value of β and changing β significantly away from the experimentally determined value of $0.24\,\mathrm{nm}^{-1}$ results in worse agreement with data. Therefore, varying β cannot explain all the observed variations from one deposition to another.

(2) Varying S changes the computed results in a systematic way, as indicated in Fig. 8 and it does help in improving agreement with some aspects (particularly the experimental saturation of $T_c \sim 9$ K), but at the expense of some other aspects such as the standard deviation.

(3) Varying ξ_{SC} for different diameters is not especially meaningful, given that the Nb purity is unlikely to vary much across a chip, and this too does not improve the agreement with theory significantly.

(4) For the smallest islands, where interactions with the products of outgassing from PMMA can be quite large, f can be quite small. Thus, one can assume values of f that are correlated with the diameter, i.e., smaller area fraction of Nb grains for smaller diameters. In fact, the black and red points in Fig. 8 correspond to this additional assumption.

Based upon simultaneous variations of these parameters within reasonable ranges, we conclude that while the extremal-grain model best explains many important aspects of our data, there are remaining disagreements that deserve further study.

Overall, the anomalous size dependence of T_c we observe in our islands of granular Nb films is explained semiquantitatively as a rare-region effect: specifically, by a model in which the onset of superconductivity on an island coincides with the transition temperature of its largest constituent grain. This "extremal-grain" model both accounts for the size dependence of the transition temperature and predicts variations in T_c for islands of fixed size. Thus, we provide evidence for rare-region effects in a system having $R \ll R_Q$.

1. Alternative models and random resistor network simulation

While the extremal-grain model does agree with much of our data, as discussed above, it is important to rule out alternative explanations, particularly because the island normal-state resistance, R_N, also scales with island diameter [Fig. 9(c)].

We first consider the role of shunting resistance and normal metal suppression from the contacts by measuring Nb islands having underlying Au films, which provide a resistive shunt across the island and greater normal metal suppression. As can be seen E2 Au of Fig. 2, the T_c's of islands with underlying Au were similar to those of islands without underlying Au, indicating that neither suppression from normal metal contacts nor shunting resistance significantly altered T_c.

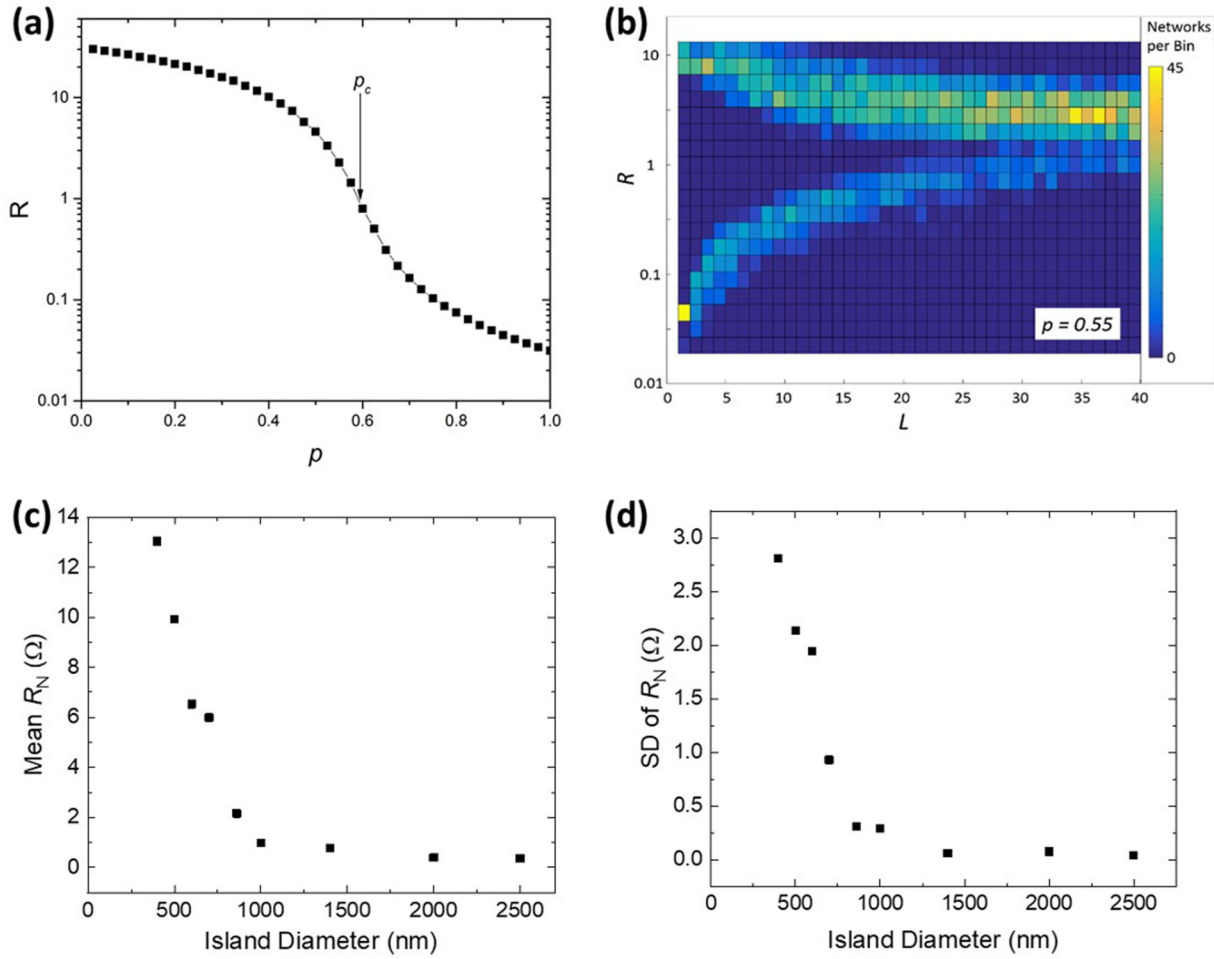

FIG. 9. Simulations of random network of resistors. (a) Resistance of a random resistor model with a probability, p, of there being a low-resistance connection rather than a high-resistance connection. (b) A histogram of resistance as a function of L, the width of a square array. The islands split into two groupings with increasing L, one with lower resistance that is spanned by a low-resistance network, and another that is split by a hole in the network. The two groupings are equal in number near p_c, but the higher-resistance grouping is dominant for $p < p_c$ and the lower-resistance grouping dominates $p > p_c$. (c) Our data for mean R_N vs island diameter for evaporation 7 (E7), clearly correspond to the $p < p_c$ case involving weakly linked network clusters. (d) Island-to-island fluctuations of R_N increase rapidly below ~700 nm, which is consistent (see text) with our random resistor network model for $p < p_c$.

The dependence of island normal-state resistance on island diameter can be best explained by transport through a highly granular material, where most of the current passes through the most conducting paths. Since fewer of these highly conductive paths are available for small diameter islands, both the mean value and the variation in R_N is greater for smaller diameter islands [Figs. 9(c) and 9(d)]. We provide the results of a simulation that uses a random percolating network [30–32] to explain, semiquantitatively, our data for the dependence of island normal-state resistance on island diameter.

Tuning the probability of a connection between adjacent nodes existing, p, and a connection not existing, $1 - p$, the random network studies observe a phase transition at a critical probability, p_c, from finite-sized clusters for $p < p_c$ to an infinite cluster of linked nodes throughout the network for $p > p_c$. The relevant length scale involved is the correlation length, $\xi \propto |p - p_c|^{-\alpha}$, where α is a scaling constant. This corresponds to the radius of the largest percolative clusters for $p < p_c$ and the radius of the largest holes in the infinite percolative cluster in $p > p_c$.

Our system corresponds more closely to the case of a good conductor in a poor conductor, which can be studied by giving the open links a large but finite resistance [33]. The resistance of this can be seen in Fig. 9(a), with a crossover near $p_c \sim 0.6$. For $p < p_c$, sample resistance is dominated by weak links between network clusters, and for $p > p_c$, the conductance is dominated by a single spanning cluster. The finite-size behavior of this model results in either a network cluster spanning the array or a hole in a network cluster dividing the array. This leads to array resistance distribution splitting as the array width, L, decreases. This splitting is shown on a logarithmic scale in Fig. 9(b) for a specific value of $p = 0.55$. Due to proximity of this p to p_c, the upper and lower curves are approximately equal in magnitude, but the lower curve is suppressed for $p < p_c$ and the upper curve is suppressed for $p > p_c$.

Since we observe increasing resistance with decreasing island diameters, our data [Fig. 9(c)] correspond to the $p < p_c$ case involving weakly linked network clusters. The relevant length scale of this system is the spacing of key current paths,

which corresponds to the size of a low-resistance network cluster. This does not correspond to a single Nb grain, which would yield finite-size effects on the scale of nanometers. Instead, the network cluster likely corresponds to clusters of grains, and that is qualitatively consistent with both the large increase in R_N [Fig. 9(c)], and also the large island-to-island fluctuations of R_N [Fig. 9(d)] below diameters of approximately 700 nm.

V. CONCLUSIONS

Our results suggest a particular physical picture of the local nature of the superconducting state near the superconductor-metal transition in this system: this state is inhomogeneous and is dominated by rare regions, as suggested in Refs. [3,34]. By exploring micron-scale systems, and by carefully correlating microstructure with modeling, we have been able to show the influence of rare regions on superconducting transport. We have found, remarkably, that even when grains are coupled strongly enough that the normal-state resistance is small, the superconducting transition can still be captured via a model of effectively decoupled "grains." In this sense, our micron-scale superconducting islands behave like many other strongly random quantum systems, such as high-temperature superconductors [35,36]. We note that the rare-region effects we have discussed are not limited to granular Nb and should appear in other disordered systems of superconducting puddles within a metallic matrix.

ACKNOWLEDGMENTS

We thank Vadim Oganesyan and Aharon Kapitulnik for helpful discussions. We also thank Mauro Sardela and James Lee for performing the XRD measurements and analysis, Scott Maclaren for assistance with conducting AFM, and Timothy Spila for performing the RBS measurements. This work was supported by the DOE Basic Energy Sciences under DE-SC0012649 and the National Science Foundation (NSF) under DMR 17-10437. S.G. acknowledges funding from the Walter Burke Institute. J.-H.K. and J.-M.Z. are supported as part of the Center for Emergent Superconductivity, an Energy Frontier Research Center funded by the US Department of Energy, Office of Science, Office of Basic Energy Sciences, under Award No. DE-AC0298CH10886. This research was carried out in part in the Frederick Seitz Materials Research Laboratory Central Research Facilities at the University of Illinois.

APPENDIX

We begin with the Landau free energy for a single superconducting grain in a metallic matrix, Eq. (1) of Spivak *et al.* [3].

$$F = -\frac{(\gamma - \gamma_c)\Delta^2}{2} + \frac{\Delta^4}{4\Delta_0^2} + \cdots .$$

For simplicity (and to avoid subtleties specific to the zero-temperature limit) we assume that the system is at some nonzero temperature that is much lower than the bulk T_c. The control parameter γ depends on the size of the grain L, because the proximity effect from neighboring metallic grains suppresses superconducting fluctuations on the anomalously large grain. The extent of this suppression depends in a complicated way on the size of the grain and the properties of the metallic grains, oxide layers, etc. [37]. For γ near the critical value γ_c, we can Taylor expand the L dependence to linear order, giving the Landau free energy

$$F = -\frac{c(L - L_c)\Delta^2}{2} + \frac{\Delta^4}{4\Delta_0^2}$$

for some constant c. Minimizing this free energy gives the result in the main text.

[1] E. Miranda and V. Dobrosavljevic, Disorder-driven non-Fermi liquid behavior of correlated electrons, Rep. Prog. Phys. **68**, 2337 (2005).
[2] D. S. Fisher, Phase transitions and singularities in random quantum systems, Physica A **263**, 222 (1999).
[3] B. Spivak, P. Oreto, and S. A. Kivelson, Theory of quantum metal to superconductor transitions in highly conducting systems, Phys. Rev. B **77**, 214523 (2008).
[4] D. Kowal and Z. Ovadyahu, Scale dependent superconductor-insulator transition, Physica C **468**, 322 (2008).
[5] M. V. Feigel'man, A. I. Larkin, and M. A. Skvortsov, Quantum Superconductor-Metal Transition in a Proximity Array, Phys. Rev. Lett. **86**, 1869 (2001).
[6] B. Sacépé, C. Chapelier, T. I. Baturina, V. M. Vinokur, M. R. Baklanov, and M. Sanquer, Disorder-Induced Inhomogeneities of the Superconducting State Close to the Superconductor-Insulator Transition, Phys. Rev. Lett. **101**, 157006 (2008).
[7] Y. Xing, H.-M. Zhang, H.-L. Fu, H. Liu, Y. Sun, J.-P. Peng, F. Wang, X. Lin, X.-C. Ma, Q.-K. Xue, J. Wang, and X. C. Xie, Quantum Griffiths singularity of superconductor-metal transition in Ga thin films, Science **350**, 542 (2015).
[8] L. Zhao, H. Deng, I. Korzhovska, M. Begliarbekov, Z. Chen, E. Andrade, E. Rosenthal, A. Pasupathy, V. Oganesyan, and L. Krusin-Elbaum, Emergent surface superconductivity in the topological insulator Sb_2Te_3, Nat. Commun. **6**, 8279 (2015).
[9] J. Biscaras, N. Bergeal, S. Hurand, C. Feuillet-Palma, A. Rastogi, R. C. Budhani, M. Grilli, S. Caprara, and J. Lesueur, Multiple quantum criticality in a two-dimensional superconductor, Nat. Mater. **12**, 542 (2013).
[10] F. M. Izrailev, A. A. Krokhin, and N. M. Makarov, Anomalous localization in low-dimensional systems with correlated disorder, Phys. Rep. **512**, 125 (2012).
[11] N. Mason and A. Kapitulnik, Dissipation Effects on the Superconductor-Insulator Transition in 2D Superconductors, Phys. Rev. Lett. **82**, 5341 (1999).
[12] M. P. A. Fisher, Dissipation and quantum fluctuations in granular superconductivity, Phys. Rev. B **36**, 1917 (1987).
[13] H. M. Jaeger, D. B. Haviland, B. G. Orr, and A. M. Goldman, Onset of superconductivity in ultrathin granular metal films, Phys. Rev. B **40**, 182 (1989).

[14] Y. Saito, Y. Kasahara, J. Ye, Y. Iwasa, and T. Nojima, Metallic ground state in an ion-gated two-dimensional superconductor, Science **350**, 409 (2015).
[15] G. Deutscher, O. Entin-Wohlman, S. Fishman, and Y. Shapira, Percolation description of granular superconductors, Phys. Rev. B **21**, 5041 (1980).
[16] O. Entin-Wohlman, A. Kapitulnik, and Y. Shapira, Dependence of T_c on the normal-state resistivity in granular superconductors, Phys. Rev. B **24**, 6464 (1981).
[17] Z. Han, A. Allain, H. Arjmandi-Tash, K. Tikhonov, M. Feigel'man, B. Sacépé, and V. Bouchiat, Collapse of superconductivity in a hybrid tin-graphene Josephson junction array, Nat. Phys. **10**, 380 (2014).
[18] A. Kamlapure, T. Das, S. C. Ganguli, J. B. Parmar, S. Bhattacharyya, and P. Raychaudhuri, Emergence of nanoscale inhomogeneity in the superconducting state of a homogeneously disordered conventional superconductor, Sci. Rep. **3**, 2979 (2013).
[19] S. Eley, S. Gopalakrishnan, P. M. Goldbart, and N. Mason, Approaching zero-temperature metallic states in mesoscopic superconductor-normal-superconductor arrays, Nat. Phys. **8**, 59 (2012).
[20] P. W. Anderson, Theory of dirty superconductors, J. Phys. Chem. Solids **11**, 26 (1959).
[21] D. C. Ralph, C. T. Black, and M. Tinkham, Spectroscopic Measurements of Discrete Electronic States in Single Metal Particles. Phys. Rev. Lett. **74**, 3241 (1995).
[22] S. Bose, A. M. García-García, M. M. Ugeda, J. D. Urbina, C. H. Michaelis, I. Brihuega, and K. Kern, Observation of shell effects in superconducting nanoparticles of Sn, Nat. Mater. **9**, 550 (2010).
[23] W.-H. Li, C. C. Yang, F. C. Tsao, and K. C. Lee, Quantum size effects on the superconducting parameters of zero-dimensional Pb nanoparticles, Phys. Rev. B **68**, 184507 (2003).
[24] S. Bose, P. Raychaudhuri, R. Banerjee, P. Vasa, and P. Ayyub, Mechanism of the Size Dependence of the Superconducting Transition of Nanostructured Nb, Phys. Rev. Lett. **95**, 147003 (2005).
[25] T. Hoss, C. Strunk, and C. Schonenberger, Non-organic evaporation mask for superconducting nano-devices, Microelectron. Eng. **46**, 149 (1999).
[26] K. Ohnishi, T. Kimura, and Y. Otani, Improvement of superconductive properties of mesoscopic Nb wires by Ti passivation layers, Appl. Phys. Express **1**, 021701 (2008).
[27] H. Bartolf, *Fluctuation Mechanisms in Superconductors: Nanowire Single-Photon Counters, Enabled by Effective Top-Down Manufacturing* (Springer, Spektrum, 2016).
[28] K. H. Kim, H. Xing, J. M. Zuo, P. Zhang, and H. F. Wang, TEM based high resolution and low-dose scanning electron nanodiffraction technique for nanostructure imaging and analysis, Micron **71**, 39 (2015).
[29] P. Dubos, H. Courtois, B. Pannetier, F. K. Wilhelm, A. D. Zaikin, and G. Schön, Josephson critical current in a long mesoscopic S-N-S junction, Phys. Rev. B **63**, 064502 (2001).
[30] A. Miller and E. Abrahams, Impurity conduction at low concentrations, Phys. Rev. **120**, 745 (1960).
[31] V. Ambegaokar, B. I. Halperin, and J. S. Langer, Hopping conductivity in disordered systems, Phys. Rev. B **4**, 2612 (1971).
[32] D. Stauffer, Scaling theory of percolation clusters, Phys. Rep. **54**, 1 (1979).
[33] J. Bernasconi, Real-space renormalization of bond-disordered conductance lattices, Phys. Rev. B **18**, 2185 (1978).
[34] D. Kowal and Z. Ovadyahu, Disorder induced granularity in an amorphous superconductor, Solid State Commun. **90**, 783 (1994).
[35] A. N. Pasupathy, A. Pushp, K. K. Gomes, C. V. Parker, J. Wen, Z. Xu, G. Gu, S. Ono, Y. Ando, and A. Yazdani, Electronic origin of inhomogeneous pairing interaction in the high-T_c superconductor $Bi_2Sr_2CaCu_2O_{8+\delta}$, Science **320**, 196 (2008).
[36] K. K. Gomes, A. N. Pasupathy, A. Pushp, S. Ono, Y. Ando, and A. Yazdani, Visualizing pair formation on the atomic scale in high-T_c superconductor $Bi_2Sr_2CaCu_2O_{8+\delta}$, Nature (London) **447**, 569 (2007).
[37] P. G. De Gennes, Boundary Effects in Superconductors, Rev. Mod. Phys. **36**, 225 (1964).